AAS 14-114

ASTROS: A 5DOF EXPERIMENTAL FACILITY FOR RESEARCH IN SPACE PROXIMITY OPERATIONS

Panagiotis Tsiotras*
School of Aerospace Engineering
Georgia Institute of Technology, Atlanta, GA, 30332-0150

In this paper we summarize the technical characteristics of the Autonomous Spacecraft Testing of Robotic Operations in Space (ASTROS) facility at the School of Aerospace Engineering at Georgia Tech. The experimental facility consists of a 5DOF platform supported on hemispherical and linear air-bearings moving over an extremely flat epoxy floor, thus simulating almost friction-free conditions. The ASTROS facility can be used to support the development and testing of autonomous rendezvous and docking (ARD) and other general proximity operations (ProxOps) algorithms. A variety of on-board sensors and actuators allow the testing of most realistic scenarios one may encounter in practice. An overhead VICON system is used to provide baseline truth data for validation purposes.

INTRODUCTION

NASA has recently identified general proximity operations, and autonomous rendezvous and docking (ARD) operations in particular, as crucial technologies that would enable a plethora of future missions in space. See, for instance, the recent Broad Agency Announcement from the Office of Chief Technologist of NASA, which identified Autonomous Rendezvous and Docking as one of the Technology Thrust areas.[1] These missions include satellite servicing and refueling, space station resupply with consumables, removal of space debris, spacecraft structural integrity inspection in Earth orbit, as well as support for deep space missions to Mars and other planets and comets. As mentioned in Refs. [2, 3], the most probable scenario for a manned mission to Mars will require ARD maneuvers both in LEO as well as in Mars orbit, just prior to the return to the Earth. Comets, in particular, represent a target undergoing complicated motion, due to outgassing effects imparting forces and moments on the rigid body. Landing on a small comet, therefore, presents several of the same challenges as rendezvousing and docking with an uncontrolled satellite. Removing decommissioned satellites from orbit ("space debris") is another example that will require extensive robust capabilities for autonomous rendezvous, grasping, and docking in space. The importance of ARD capabilities for these and other scenarios to NASA's mission was already stressed in Ref. [4] and reaffirmed, more recently, in Ref. [5].

The US Air Force has also identified proximity operations in space as one of the key technologies for maintaining superiority in space. Proximity operations will enable routine servicing and refueling of satellites. They can help with the protection of friendly space assets against an adversary, or with the monitoring of an adversary's space assets, especially in the geosynchronous orbit (GEO). At nearly 25,000 miles high, objects in GEO are too small to be easily seen optically or by radar. A small service vehicle deployed in the proximity of a target satellite can provide accurate informa-

*Dean's Professor, AIAA Fellow, Email: tsiotras@gatech.edu.

tion of the satellite's structural health or (if the target is unknown) identify and categorize the target satellite.

Despite the importance of ARD technology in enabling a wide plethora of space missions (both civilian and military), it is rather surprising that US capabilities in this technology area are somewhat lagging; in many respects they are considered behind the Russian and European ARD capabilities.[2] This is mainly owing to historical reasons, going back to the 1960's, resulting from the different philosophies followed by the US and the Russian space programs from the early beginning. While the US Gemini and Apollo programs focused on manned space exploration, the Russian Cosmos missions were unmanned. Since then, in all of the American missions, human pilots were in the vehicle control loop during rendezvous and docking, while the Russians used a primarily automated approach with the pilots having a supervisory role.[6] Recognizing this deficiency, there has been a renewed interest in autonomous rendezvous, docking and proximity operations in space from a number of agencies in the US (e.g., DARPA's Orbital Express and Phoenix programs, NASA's DART and STORMM missions, AFRL's XSS-11 flight experiment, etc).

A crucial element in advancing ARD and ProxOps state-of-the-art is the ability to test new relative navigation and guidance algorithms, grasping algorithms, vision processing and perception algorithms etc that can support ProxOps in orbit. In contrast however to other related fields (e.g., unmanned aerial or ground vehicles), testing navigation, perception and guidance algorithms for space proximity operations is hindered by the difficulty of routinely and cheaply testing these algorithms in a realistic environment. Recognizing this drawback (which stifles or delays the transitioning of new theoretical and technological advances to actual spacecraft systems), several agencies (both in industry and academia) have recently invested in the development of test facilities for experimental testing of spacecraft proximity operations in a 1-g environment.[7–15] For a nice and comprehensive review of spacecraft simulator facilities up to the time of its publication, see also Ref. [16].

In this paper we summarize the efforts undertaken at the Georgia Institute of Technology to establish a testbed that can be used for academic research related with ARD and ProxOps in space.

MAIN PLATFORM DESCRIPTION

The Georgia Tech main facility is based on an a 5DOF experimental platform consisting of a lower and an upper stage. The main structure of the ASTROS is the upper stage, whose main operational characteristics can be found in Refs. [17] and [18] and which are briefly summarized below.

The lower stage consists of four high-pressure air storage vessels (three external and visible in Figure 1 and a smaller one inside the pedestal), three linear air-bearing pads, a hemi-spherical air-bearing cup, and dedicated electronics that drive the solenoid valves for each air-bearing. The three external vessels have a total volume of 3000 in^3, while the internal vessel has a volume of 360 in^3. The vessels are connected in series and are filled with compressed air at 3295 psi to provide air to both the linear and hemi-spherical air-bearings.

Each linear air pad is able to levitate about 175 lbf load at an operating pressure of 25 psi. The maximum load of the hemi-spherical air-bearing is approximately 350-400 lbf at 80 psi air pressure, which is sufficient to support the upper stage. A series of high-pressure and low-pressure regulators and accompanying safety valves ensure that air flow is supplied continuously to all air-bearings at the appropriate pressure level. The three linear air pads allow the lower stage to float on a very thin (air gap about 70-80 microns) cushion of air. The minimum air gap is dictated by the total weight

of the platform and the maximum air flow rate and maximum pressure through the three linear air bearings.

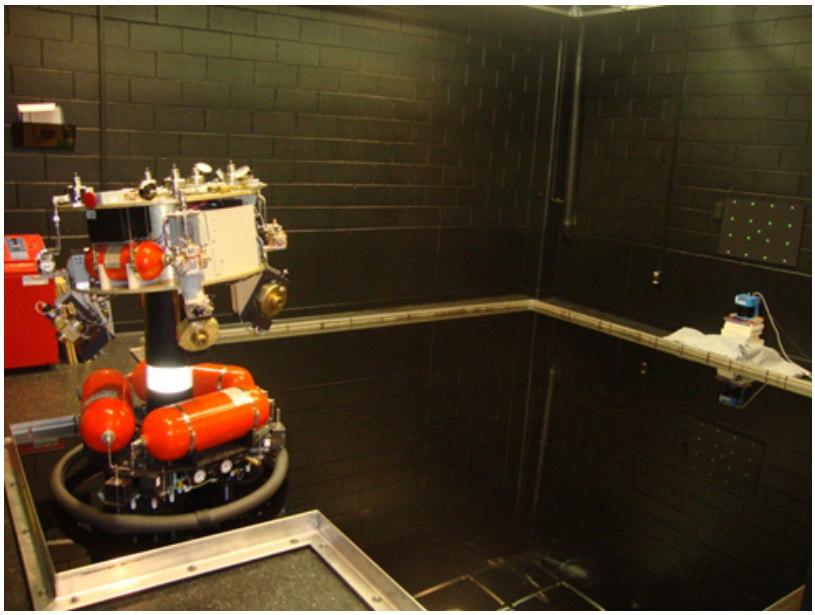

Figure 1 Experimental platform and test area.

All air-bearings are either remotely controlled by the on-board computer or are manually operated via external switches. There are three different operation modes, which allow one to selectively open and close the valves for a 3-dof translational/rotational mode with heading change (only lower platform levitated), full 3-dof rotational mode (only upper platform levitated), and full 5-dof translational/rotational mode (both upper and lower platforms levitated). This provides great flexibility for the type of experiments one may conduct using the ASTROS.

Sensors and Actuators

The upper stage simulates a typical spacecraft "bus" and is made of a two-level brass structure that is supported on a hemi-spherical air bearing, allowing rotation of the upper stage with respect to the supporting pedestal about all three axes ($\pm 30 \text{ deg}$ about the x and y axes and a full rotation about the z axis). Two 225 in^3 high-pressure (at 2000 psi) vessels are used to store cold-nitrogen gas or compressed air for the operation of the on-board thrusters. The platform has 12 thrusters in clusters of three, installed on the platform in a 3-3-3-3 configuration, each thruster providing a maximum of 5 N of force. A solenoid valve operates the activation of each thruster. Each solenoid valve is driven by an amplified digital signal from the on-board control computer, with a minimum operational pulse of 15 ms, which corresponds to a bandwidth of the thruster of about 67 Hz. The thruster module allows the implementation of continuous torque via Pulse Width Pulse Modulate (PWPM) operation. A separate thrust allocation mechanism (see below) is used to schedule the thrust firings in order to achieve user-commanded force and torque histories.

Additional moments on the platform are provided by four Variable-Speed CMGs (VSCMGs) which are arranged in a conventional inverted pyramid configuration and are used to provide fine attitude control. These VSCMGs can be operated either as reaction wheels (RW mode), as con-

ventional single-gimballed CMGs (CMG mode) or simultaneously as reaction wheels and CMGs (VSCMG mode). In VSCMG/CMG mode a geared motor allows accurate gimbal rate control with resolution of 0.5 deg/sec. The maximum commanded gimbal rate is 25 deg/sec whereas the maximum wheel speed is 4000 rpm/s and the maximum wheel acceleration is about 700 rpm/s. These values correspond approximately to 770 mNm and 283 mNm torque per axis in CMG and RW mode, respectively. Slip rings allow full rotation of the gimbals about their respective axes. The on-board attitude sensors include an inertial measurement unit (IMU), a two-axis Sun/star sensor, a three-axis magnetometer and a three-axis rate gyro (RG02-3201 by Humphrey).

An on-board PC computer runs Mathworks' xPC Target real-time environment with supporting AD/DA and I/O boards, and is responsible for collecting the sensor data and implementing the control algorithms and for providing the control commands to the actuators. An additional PC-104-based computer (EPM-32 Cheetah from VersaLogic) running Ububtu version of Linux is used to process the data collected by the on-board cameras. Two cameras are installed on-board the platform, a typical color CCD camera and a LiDAR-like range camera (SwissRanger SR-3000 by MESA Imaging). The latter camera provides a 3D point cloud along with 2D normal intensity images with a depth map in real-time at video frame rates. The camera uses 55 infrared LEDs emitting amplitude modulated waves (850 nm) at 20 MHz and calculates the amplitude and phase shift of the reflected wave at each pixel to determine intensity and range information.

All on-board electronics are powered by two rechargeable lithium-iron batteries. An ethernet wireless router provides communication between the main control computer and the vision computer via an ad-hoc LAN as well as wireless communication with the host computer.

The schematic of the overall interconnections are shown in Figure 2.

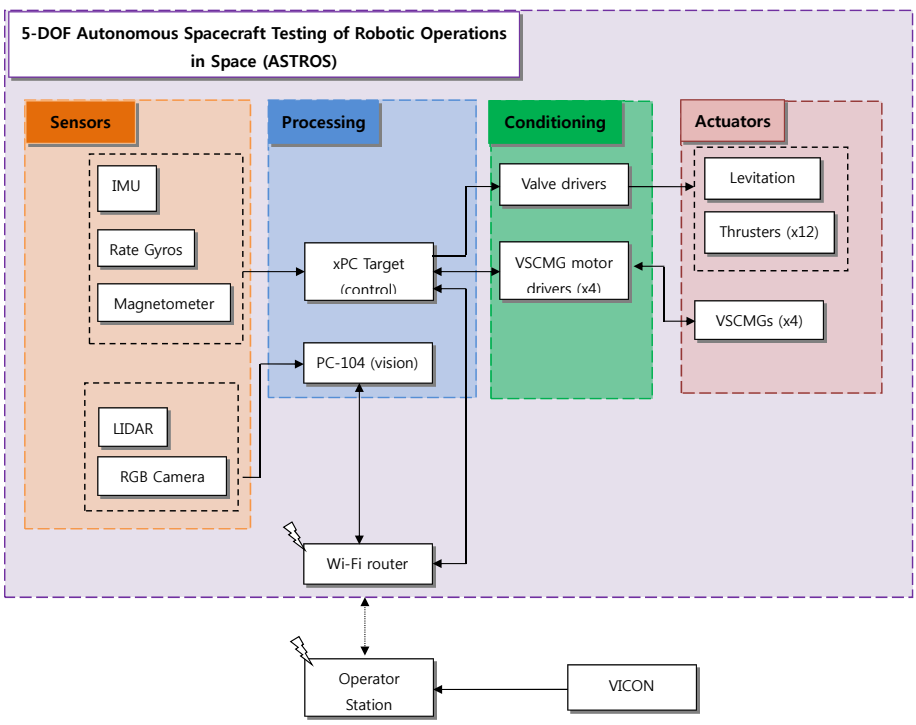

Figure 2 Schematic diagram of sensor and actuator configuration and their interconnections.

Thruster Allocation Strategy

In order to generate the required force and torque commands using the twelve thrusters a linear program subject to constraints is solved in order to select the thrusters to be fired and the order at which they are fired. This is a well-known thruster allocation program and several algorithms exist in the literature for its solution.[19,20] The upper stage of the ASTROS platform is equipped with 12 thrusters, with four thrusters aligned along each of the three body axes. However, owing to the location of each thruster with respect to the center of rotation, firing each thruster causes not only translational motion but also coupled rotational motion. The thruster allocation strategy compensates for any unwanted torque components by firing the necessary combination of thrusters.

In the ASTROS implementation this linear constrained optimization problem is efficiently solved using the simplex method assuming that the exact location and thrust level of each thruster is known. A C++ code was written and implemented as an S-function in the Matlab/Simulink® environment with the help of GNU Linear Programming Kit (GLPK).[21]

EXPERIMENTAL ARENA

The 5-dof platform is free to translate on a very flat epoxy floor with the help of three linear air-bearings in order to simulate almost friction-free conditions. A schematic of the arena is shown in Figure 8(a). The arena floor includes the operational area ($156" \times 168"$) and the stationary/parking area ($40" \times 58"$). A cushiony rail at the outer edge of the floor protects the platform during soft collisions. An overhead projector installed on the ceiling can be used to project virtual images from Earth orbit against a giant projection screen located on the room South wall (Figure 3).

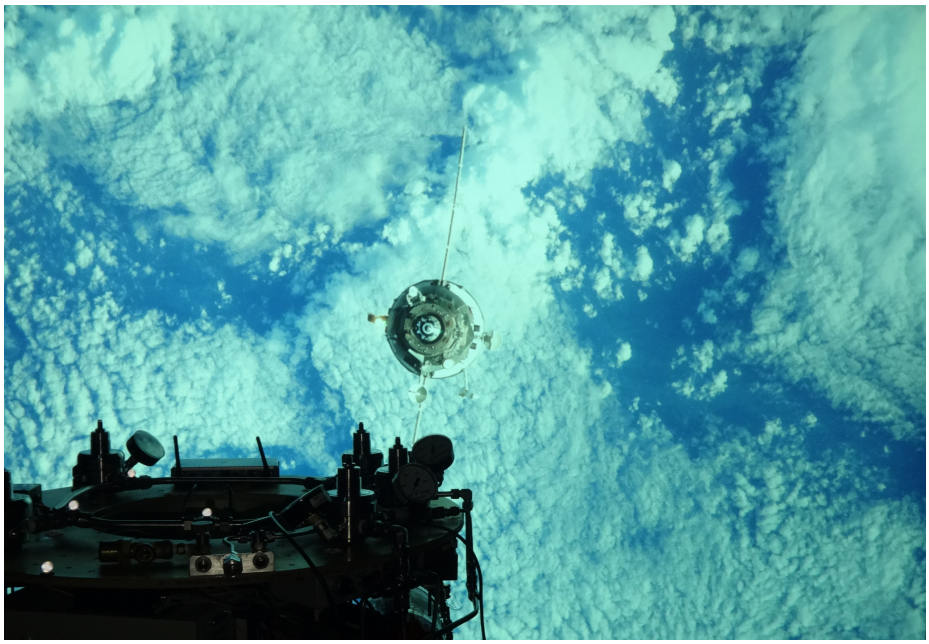

Figure 3 A large projection screen is used to simulate virtual Earth orbit scenarios. Part of the ASTROS upper stage platform is visible at the left bottom corner.

Despite the very tight tolerances regarding the flatness of the experimental arena, construction imperfections result is local undulations and gradients that impart small (but noticeable) linear ac-

celeration to the platform because of gravity. These have to be modeled in simulations and compensated, if needed, during the experiments. Therefore a floor height map $f(x, y)$ was constructed by taking measurements at several places of the arena using an inclinometer. A cubic interpolation of the data was applied in order to have gradients for every 1 inch along the x and y directions. Then, the interpolated gradient map is integrated with respect to x and y using a trapezoidal rule. The result is shown in Figure 4.

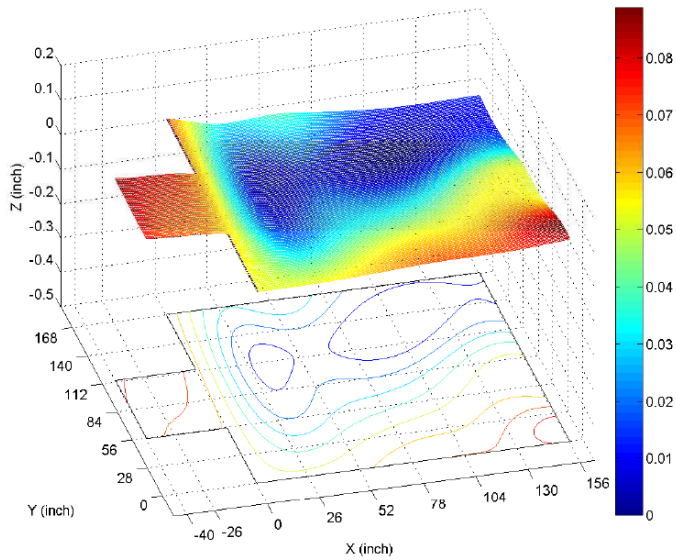

Figure 4 Floor height map of experimental arena.

The accelerations can be computed using the expressions

$$a_{g_\star} = -\frac{g \tan \theta_\star}{1 + \tan^2 \theta_\star}, \qquad \star = x, y, \tag{1}$$

where θ_x and θ_y are the local floor slopes at the point (x, y) measured by the inclinometer. The magnitude of the acceleration is between 1.77×10^{-5} m/sec^2 and 6.7×10^{-3} m/sec^2 with a median of 3.84×10^{-3} m/sec^2. This gravity-driven disturbance acceleration to the platform is implemented in a Simulink® as a lookup table of the interpolated gradients.

Three high-pressure gas bottles rated up to 6000 psi are used for air storage. They are used to recharge the on-board tanks, and they can also be utilized to provide air to the platform during the experiments, if needed. A 5000 psi high pressure air compressor (90SE-5000 from Max-Air, shown in Figure 5(a)) is utilized to fill the bottles. Additional low-pressure shop air supply is also available. Dehumidifier filters clean the shop air, and provide dry air to the platform via an umbilical when the on-board tanks are depleted. The on-board gas tanks for the on-board thruster reaction control system (RCS) are charged using two additional nitrogen gas bottles (see Figure 5).

LOCALIZATION SYSTEM

An aluminium grid attached on the ceiling over the experimental area allows the mounting of several equipment. In addition to two Pan/Tilt/Zoom color video cameras (Sony BRC-300) that providing wide-angle, live-view of the experimental arena, a VICON® motion capture system has

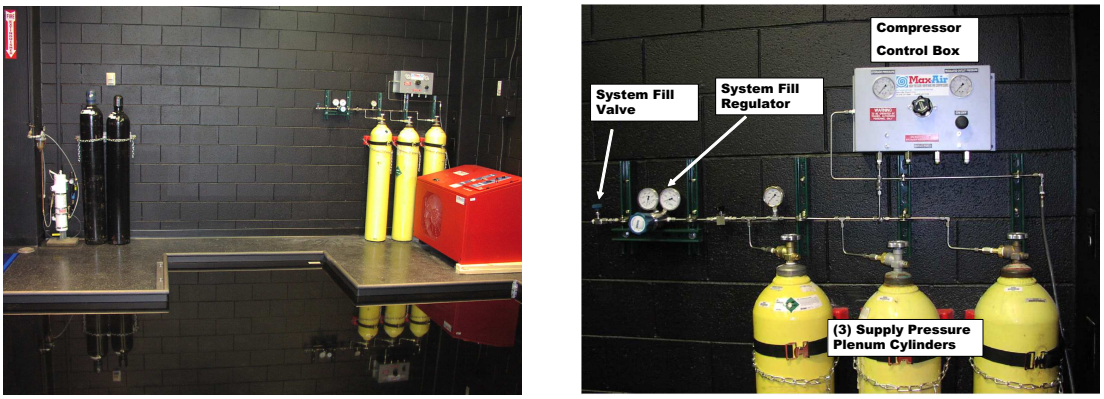

(a) A view of the compressed air filling system.

(b) The high pressure charging station.

Figure 5 The compressed air filling system consists of a high pressure air compressor on the right of the left picture, three high-pressure gas bottles, two cold-nitrogen gas bottles, a charging station, and an air dehumidifier for the shop air.

been installed on the aluminum grid to provide accurate localization and attitude information with respect to an inertial frame. The VICON system consists of eight Bonita B10 cameras shown in Figure 6(a), each having a resolution of one megapixel and maximum frame rate of 250 Hz. The cameras track six reflective markers attached on the upper stage of the ASTROS platform.

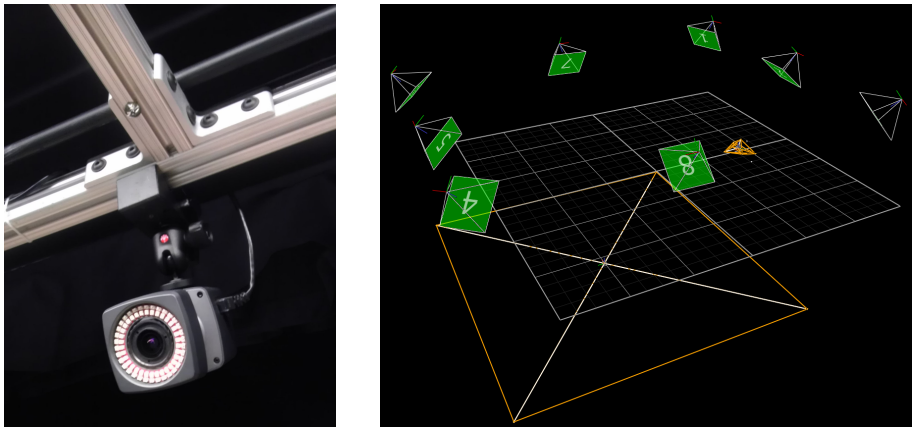

(a)

(b)

Figure 6 (a) VICON® Bonita B10 camera mounted on ceiling grid; (b) Experimental area as seen by the motion capture software.

The cameras are connected through a Power-Over-Ethernet (POE) switch to the control room host computers. A dedicated software on these computers is used to process the VICON measurements and determine the translation and rotation of the upper stage with respect to the experimental area (see Figure 6(b)). After calibration, the VICON system delivers sub-millimeter and sub-degree accuracy.

A second, independent localization system using a SICK LMS200 laser sensor[22] has been developed to provide accurate inertial position information of the platform. The laser sensor is installed on the West wall of the experimental arena (see Figure 1). Using a system of mirrors and electrical

motors, the SICK laser sensor sweeps a maximum angular range of 180 deg with a maximum angular resolution of 0.25 deg. All measurements are taken within the same 2-D plane. Figure 7 shows a typical scan output from the laser sensor.

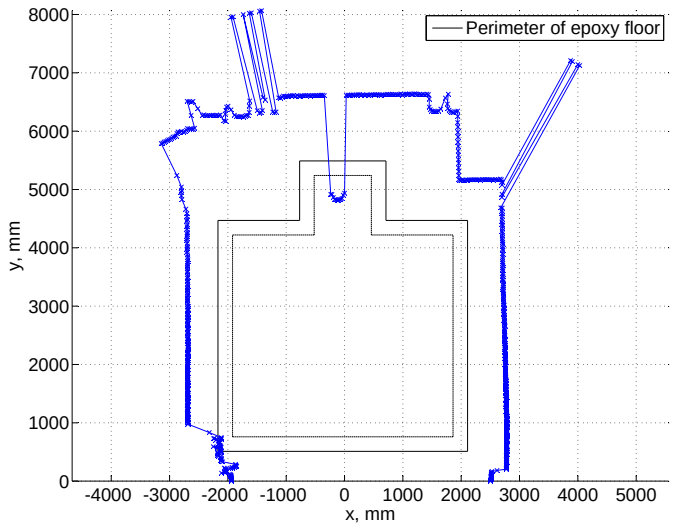

Figure 7 Cloud of points measured by the SICK LMS200 2D laser scanner. The SICK laser scanner is install against the West wall of the experimental arena (bottom of figure, at the origin of the axes system).

Since we are only interested in the points that fall inside the epoxy floor perimeter, all points falling outside the dashed virtual perimeter shown in Figure 7 are discarded. The cylindrical pedestal is measured by the SICK LMS200 as a collection of points forming an almost perfect semicircle. A least-squares algorithm[23] has been used to fit a circle to these data points in order to retrieve the coordinates of the center of the pedestal. A reflective band on the pedestal (clearly shown in Figure 1) helps the collection of good quality measurements. The final algorithm exhibits millimeter-level accuracy at a measurement frequency approximately 2 Hz.

CONTROL ROOM

The monitoring of all experiments is conducted from a separate control room separated from the experimental area via a wall. Three large windows allow the observation of the experiments from the control room. Figure 8(b) shows a picture of the control room. Two overhead Sony BRC-300 PTZ cameras are used to provide live video from the experimental area. The experiments can be remotely operated and managed through several host computers equipped with standard software tools, e.g., Matlab/Simulink®. The computers communicate with the ASTROS on-board control computer using a wireless high-speed link. Three 46” LCD overhead displays and an overhead projector are used to display the data collected during the experiments. A switch matrix enables the distribution of the video feeds from the different sources (on-bard cameras, PTZ overhead cameras, and computer monitors) to the three LCD displays or the overhead projector.

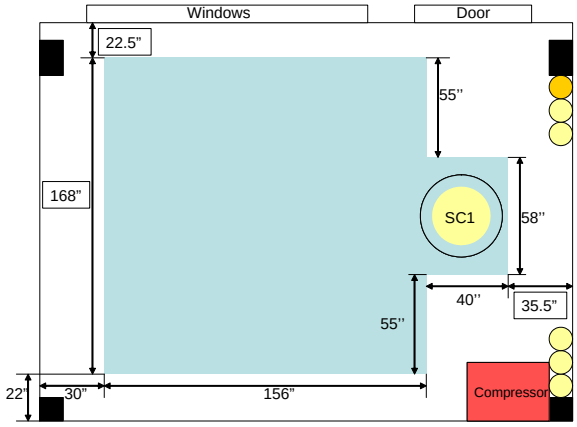

(a) Schematic of the experimental arena.

(b) Control room.

Figure 8 Schematic of test experimental arena and control room.

RELATIVE POSE ESTIMATION WITH A COOPERATIVE TARGET

The main objective of the ASTROS is to test vision-based pose estimation, localization and relative navigation and guidance algorithms for spacecraft executing proximity operations in space. In this section we provide some of the details of the processing pipeline currently under investigation for achieving efficient, accurate and robust relative pose estimation with a cooperative target spacecraft using a monocular camera. For more details, the interested reader is referred to Ref. [24].

In a cooperative satellite ProxOps scenario, the objective is to achieve vision-based, relative navigation about a target satellite using a known pattern placed on the target satellite. The known target, if properly designed can help achieve precise relative navigation when the target pattern is in view. However, the pattern may come in and out of view depending on the maneuvers performed by the chaser satellite. The system must therefore be capable of detecting and locking onto the pattern throughout the engagement scenario, as well as recognizing when the pattern has been lost. Additional challenges involve the fact that pattern detection needs to be invariant to relative orientation about the optical axis, insensitive to the distance to target, and somewhat robust to the perspective distortion caused by angled views of the pattern. Furthermore, the pattern itself should provide sufficient information to estimate relative pose. In addition, owing to the typically limited computational resources available in space, the processing pipeline should be computationally efficient, while at the same time being robust to uncertainty in terms of the measurements and the relative geometry.

The proposed processing pipeline, shown in Figure 9, consists of the following three key components: (a) a robust pattern detector based on an adaptive, parameterized, piecewise approximation to the Laplacian of Gaussian (LoG); (b) a joint frame-to-frame data association and relative pose estimation solver using robust point-set registration with Gaussian mixture models; and (c) an incremental smoothing algorithm that temporally smooths the pose estimates, and which provides higher accuracy over traditional recursive filtering methods given the same computational overhead.[25] The motivation for this approach is motivated from the need of a robust algorithm having reduced computational complexity that can be implemented on-board the satellite with limited computational resources.

Typically, each component in the monocular vision-based relative pose estimation pipeline op-

erates in an open-loop fashion, where one output feeds to the next input. There is no feedback of information from a later stage to an earlier stage. One of the novelties of the proposed processing framework is that includes an information feedback loop, whereby the pose estimates are fed back to the detection step to improve the target pattern detection reliability, which then impacts future pose estimates.

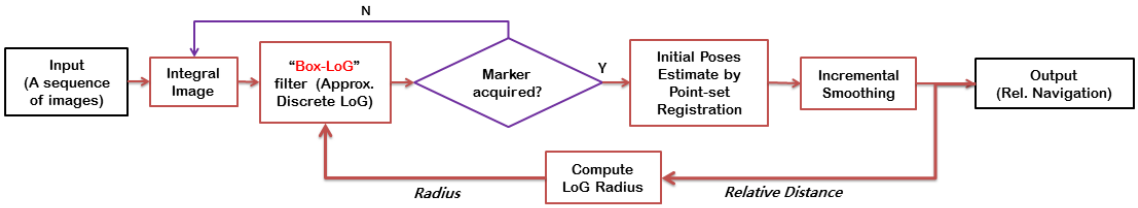

Figure 9 Overall schematic of proposed approach for cooperative relative pose estimation and visual tracking.

The landmark pattern used on the target satellite, shown in Figure 10, satisfies the following properties: (a) the pattern elements are robust at multiple scales; (b) it is co-planar so that rapid pose estimation can be achieved through homographic geometry; (c) it has a sufficient number of pattern elements to ensure well-posed pose estimation; and (d) is has a non-symmetric and non-collinear topology in order to avoid degeneracy in pose estimation and pose ambiguity due to rotations or perspective foreshortening. More details about the pattern and its desirable characteristics are given in Ref. [24].

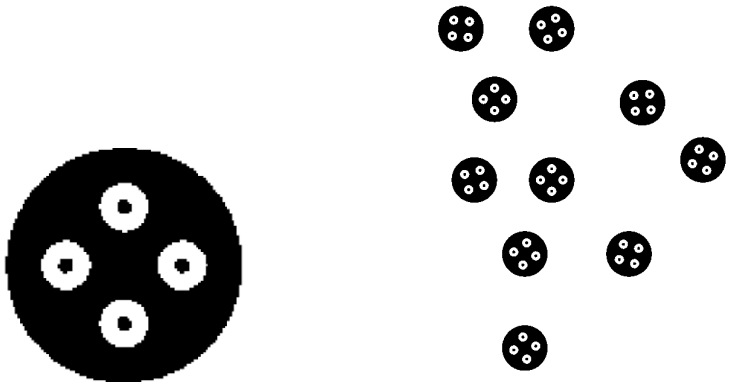

(a) Proposed pattern element. (b) Candidate pattern.

Figure 10 Pattern element and landmark pattern for cooperative visual tracking.

The framework shown in Figure 9 has been tested on ASTROS. The results are shown in Figure 11. In this figure the camera follows the (green) trajectory. The platform trajectory includes translation, rotation, and loss of view of the target pattern. At time between poses No. 37 and No. 38, there are three camera image measurements for which the pattern is out of the view of the camera meaning that the pattern is not imaged.

During the detection step, at the beginning of the test, the big marker dots of the target (see Figure 10) are detected first. As the camera approaches the target, by adapting the radius of the

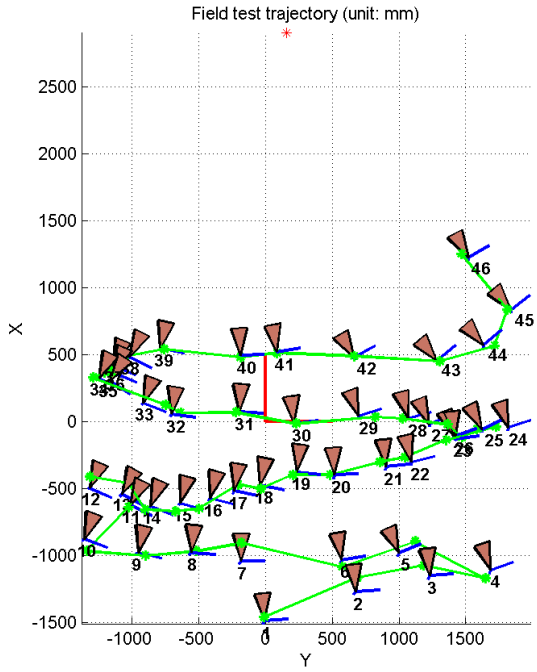

Figure 11 The ground-truth trajectory (in green) of the camera, the target position (in red star) and the final estimated camera poses (depicted by the camera objects).

detector according to the feedback from the pose estimation, the detection is switched to detect the markers of smaller size.

The detection result is illustrated in Figure 12. Once detection is ensured, the pattern target is claimed to have been acquired if the number of the detected markers is the same as the real number on the designed pattern. If the pattern is acquired, the data association and initial poses estimation is performed. Figure 13 shows an example result from the data association step, in which the target detection from the current frame is associated with the previous frame. The red crosses in the figure stand for the detection from the current frame, and the green dots are the transformed locations of the current frame detection on the previous frame under the recovered homography map. The final result is given by the final smoothed poses.

The smoothed pose estimates are depicted by the camera objects shown in Figure 11. Comparing the estimated and smoothed states to the ground-truth states for both experiments leads to the error plots in Figure 14. The relative errors of the smoothed position estimations are all smaller than 2.8%. The angle deviation between the final estimate rotation matrices and the ground-truth matrices are within $18°$. These experiments confirm the ability of the system to detect and adaptively track the target pattern, as well as to estimate the relative pose of the chaser satellite using the known planar geometry of the pattern elements.

Current research is focused on developing, testing and implementing algorithms for inspection and tracking of a tumbling target in space, when no prior information about the target satellite is assumed. No prior information about the target satellite here means that we assume no reliable pre-existing information about the shape, mass properties (inertia matrix, center of mass) or appearance of the target satellite, and no pre-existing recognizable reference markers exist on the target satellite, which could assist during the approach and docking phases. Our emphasis on non-cooperative

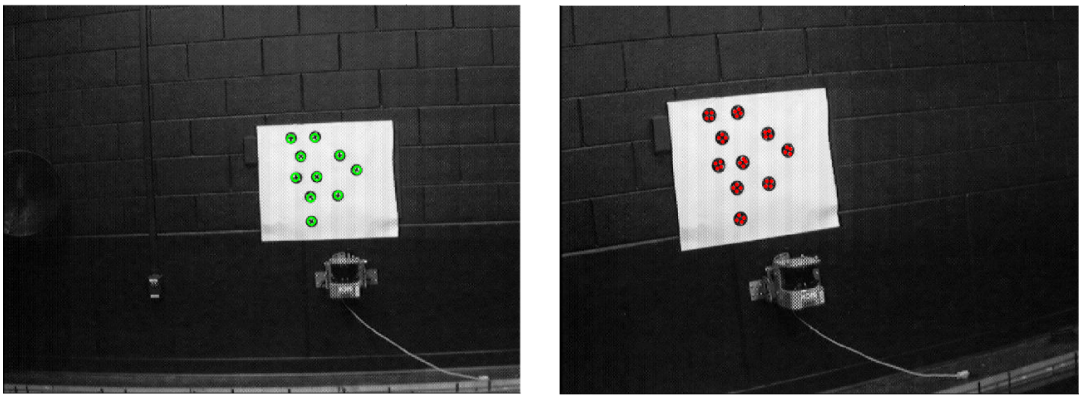

Figure 12 Detection results from field experiment.

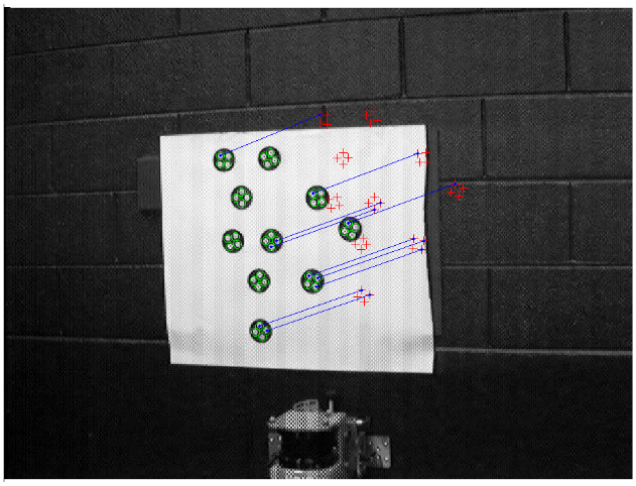

Figure 13 Data association.

target satellites stems from the greater generality and greater importance this particular problem encapsulates in terms of applications. Indeed, most of the satellites to date are not fitted with distinct features and/or sensors that can assist in an ARD scenario with a service satellite. The majority of "space debris" fall into this category. Furthermore, landing on small comets or asteroids is also a problem that can be cast as a rendezvous and docking problem with a non-cooperative target. Finally, there is a more practical reason one would like to develop the necessary ARD technology that can handle non-cooperative targets, namely, robustness. That is, the system must robust enough so that it can even accommodate cases when the attitude sensing and/or control system of the target satellite has failed and the target is tumbling. Again, most satellites that require service and/or removal from orbit will fall into this category. A scaled mockup of the second generation TDRS satellite (see Figure 15) has been built and is used as the target satellite.

CONCLUSIONS

In this paper we provide a short description of the ASTROS air-bearing test facility at the School of Aerospace Engineering at Georgia Tech. The facility is used to test the feasibility of novel vision-based relative pose estimation and relative guidance algorithms suitable for proximity operations

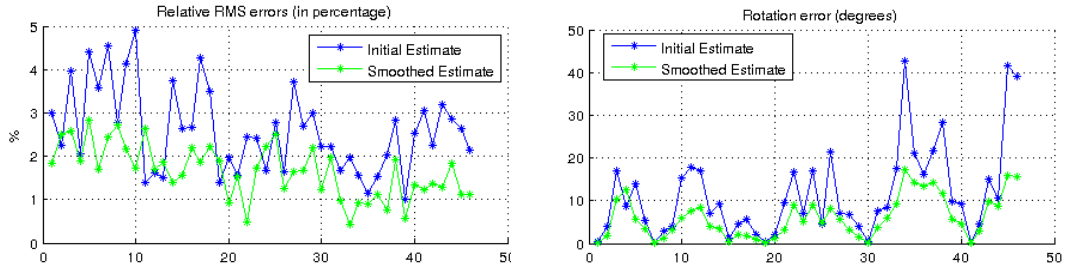

(a) (b)

Figure 14 (a) Relative errors of the estimated positions; (b) Rotation errors.

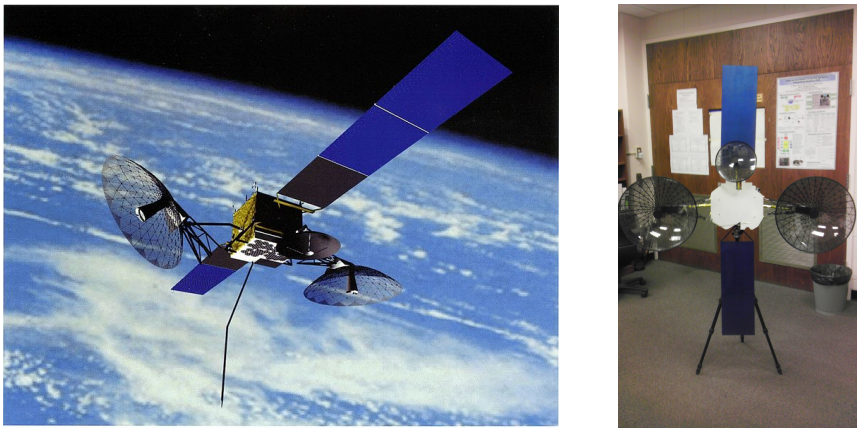

(a) (b)

Figure 15 (a) The Tracking and Data Relay Satellite (TDRS); (b) Scaled mockup of TDRS used as the target satellite for non-cooperative ProxOps scenarios.

involving small spacecraft in orbit. Autonomous target acquisition, tracking and final approach phases can all be tested using the facility. Experimental results from a new vision-based relative pose estimation algorithm using a monocular camera are also presented.

Acknowledgment

The experimental facility described in this paper has been made possible via the financial support from AFOSR DURIP awards no. FA F49620-01-1-0198 and FA9550-06-1-0379, AFRL award no. FA9453-13-C-0201, and the generous support provided by the College of Engineering at Georgia Tech. The author would also like to thank all former and current students that were instrumental in setting up the ASTROS experimental facility: Byungmoon Kim, Dongwon Jung, David Chanin, Mark Hunkele, Dae-Min Cho, Nuno Filipe, Guangcong Zhang, Michael Kontitsis.

REFERENCES

[1] "NASA Teaming Opportunity to Develop Autonomous Rendezvous and Docking Technology Demonstration Mission," http://www.spaceref.com/news/viewsr.html?pid=36516 (on-line).

[2] Polites, M. E., "Technology of Automated Rendezvous and Capture in Space," *Journal of Spacecraft and Rockets*, Vol. 36, No. 2, 1999, pp. 280–291.

[3] Vandenberg, F. A., "Autonomous Rendezvous and Docking in Mars Orbit," *Astrodynamics Specialist Conference*, Nassau, Bahamas, July 28–30 1975, Paper AAS 75-070.

[4] Quintero, R., Montgomery, R. C., and Tchoryk, P., "Autonomous Rendezvous and Docking Scenarios for the Development of Guidelines and Standards," *AIAA Space Programs and Technologies Conference and Exhibit*, Huntsville, AL, 1993, Paper AIAA 93-4753.

[5] Ambrose, R., Wilcox, B., Reed, B., Matthies, L., Lavery, D., and Korsmeyer, D., "Robotics, Tele-Robotics and Autonomous Systems Road Map: Technology Area 04," (on-line), November 2010, http://www.nasa.gov/pdf/501622main_TA04-Robotics-DRAFT-Nov2010-A.pdf.

[6] Polites, M. E., "An Assessment of the Technology of Automated Rendezvous and Capture in Space," Tech. Rep. NASA/TP-1998-208528, NASA Marshall Space Flight Center, July 1998.

[7] Romano, M., "Laboratory Experimentation of Autonomous Spacecraft Proximity-Navigation using Vision and Inertia Sensors," *AIAA Guidance, Navigation, and Control Conference and Exhibit*, San Francisco, CA, 2005.

[8] Gallardo, D., Bevilacqua, R., and Rasmussen, R. E., "Advances on a 6 Degrees of Freedom Testbed for Autonomous Satellites Operations," *AIAA Guidance, Navigation, and Control Conference*, Portland, OR, Aug. 8–11 2011, AIAA Paper 2011-6591.

[9] Romano, M., Friedman, D. A., and Shay, T. J., "Laboratory Experimentation of Autonomous Spacecraft Approach and DocDock to a Collaborative Target," *Journal of Spacecraft and Rockets*, Vol. 44, No. 1, January-February 2007, pp. 164–173.

[10] Ustrzycki, T., Lee, R., and Chesser, H., "Spherical Air Bearing Attitude Contrll Simulator for Nanosatellites," *AIAA Modeling and Simulation Technologies Conference*, Portland, OR, Aug. 8-11 2011, AIAA Paper 2011-6272.

[11] Cho, S., Shen, J., McClamroch, H., and Bernstein, D. S., "Equations of Motion for the Triaxial Attitude Control Testbed," *40th IEEE Conference on Decision and Control*, Orlando, FL, December 2001, pp. 3429–3434.

[12] Regehr, M. W., Acikmese, A. B., Ahmed, A., Aung, M., Clark, K. C., MacNeal, P., Shields, J., Singh, G., Bailey, R., Bushnell, C., et al., "The Formation Control Testbed," *IEEE Aerospace Conference*, Vol. 1, Big Sky, MT, March 6–13 2004.

[13] Ledebuhr, A. G., Ng, L. C., Jones, M. S., Wilson, B. A., Gaughan, R. J., Breitfeller, E. F., Taylor, W. G., Robinson, J. A., Antelman, D. R., and Nielsen, D. P., "Micro-Satellite Ground Test Vehicle For Proximity And Docking Operations Development," *IEEE Aerospace Conference*, Vol. 5, Big Sky, MT, March 10–17 2001, pp. 2493–2504.

[14] Jian, X., Gang, B., QinJun, Y., and Jun, L., "Design And Development Of A 5-Dof Air-Bearing Spacecraft Simulator," *International Asia Conference on Informatics and Control, Automation and Robotics*, Bangkok, Thailand, Feb. 1–2 2009, pp. 126–130.

[15] Nolet, S., Kong, E., and Miller, D. W., "Ground and Flight Testing of Multiple Spacecraft Control on SPHERES During Close Proximity Operations," *Journal of Spacecraft and Rockets*, Vol. 46, No. 6, 2009.

[16] Schwartz, J. L., Peck, M. A., and Hall, C. D., "Historical Review of Air-Bearing Spacecraft Simulators," *Journal of Guidance, Control, and Dynamics*, Vol. 26, No. 4, 2003, pp. 513–522.

[17] Jung, D. and Tsiotras, P., "A 3-DoF Experimental Test-Bed for Integrated Attitude Dynamics and Control Research," *AIAA Guidance, Navigation, and Control Conference*, Austin, Texas, 2003, AIAA 2003-5331.

[18] Cho, D., Jung, D., and Tsiotras, P., "A 5-dof Experimental Platform for Spacecraft Rendezvous and Docking," *Infotech@Aerospace Conference*, April 6–9 2009, Seattle, WA.

[19] Garus, J., "Optimization of Thrust Allocation in the Propulsion System of an Underwater Vehicle," *International Journal of Applied Mathematics and Computer Sciences*, Vol. 14, No. 4, 2004, pp. 461–467.

[20] Servidia, P. A. and Pea, R. S., "Spacecraft Thruster Control Allocation Problems," *IEEE Transactions on Automatic Control*, Vol. 50, No. 2, Feb. 2005, pp. 245–249.

[21] Makhorin, A., "GNU Linear Programming Kit," Electronic, http://www.gnu.org/software/glpk/.

[22] SICK AG, G., *Quick Manual for LMS Communication Setup*, March 2002, Version 1.1.

[23] Umbach, D. and Jones, K., "A Few Methods for fitting Circles to Data," *IEEE Transaction on Instrumentation and Measurement*, Vol. 52, No. 6, December 2003, pp. 1881–1885.

[24] Zhang, G., Vela, P., Tsiotras, P., and Cho, D.-M., "Efficient Closed-Loop Detection and Pose Estimation for Vision-Only Relative Localization in Space with a Cooperative Target," *AIAA Space and Astronautics Forum and Exposition*, San Diego, CA, August 4–7 2014.

[25] Strasdat, H., Montiel, J. M. M., and Davison, A. J., "Visual SLAM: Why filter?" *Image and Vision Computing*, Vol. 30, No. 2, 2012, pp. 65–77.